文章编号： 1007-8827(2018)05-0402-07

以氯化铵为成孔助剂两步法制备玉米芯基活性炭

魏庆玲[1,2]， 陈志敏[1]， 王晓峰[1]， 杨晓敏[1]， 王子忱[1]
(1. 吉林大学 化学学院,吉林 长春 130012;
2. 吉林化工学院 应用化学系,吉林 吉林 132022)

摘 要： 采用玉米芯为原料，氯化铵为成孔助剂，KOH 为活化剂，经水热法制备出活性炭。考察制备条件对活性炭碘值和产率的影响,并采用 SEM，TG 和 XRD 等手段对材料进行表征。结果表明,氯化铵的加入有助于活性炭多孔结构的形成。以氯化铵作为成孔助剂所制玉米芯基活性炭电极的比容量为 175 $F\cdot g^{-1}$，电流密度由 0.5 $A\cdot g^{-1}$ 升至 20 $A\cdot g^{-1}$ 时，电极的容量保持率为 73.0%；在 10 000 圈的恒流充放电过程中，比容量由 175 $F\cdot g^{-1}$ 降至 173 $F\cdot g^{-1}$。

关键词： 玉米芯；水热法；氯化铵；活性炭；电化学性能
中图分类号： TQ127.1+1 **文献标识码：** A

基金项目:国家自然科学基金(51502108);吉林省发改委自主创新能力专项基金(2014N145);吉林省科技发展计划项目(20150520016JH).

通讯作者:杨晓敏,博士,副教授. E-mail:xmyang@jlu.edu.cn
作者简介:魏庆玲,硕士,副教授. E-mail:wqlrose1999@163.com

A two-step method for the preparation of high performance corncob-based activated carbons as supercapacitor electrodes using ammonium chloride as a pore forming additive

WEI Qing-ling[1,2], CHEN Zhi-min[1], WANG Xiao-feng[1], YANG Xiao-min[1], WANG Zi-chen[1]
(1. *College of Chemistry, Jilin University, Changchun* 130012, *China*;
2. *Department of applied chemistry, Jilin Institute of Chemical Technology, Jilin* 132022, *China*)

Abstract: Activated carbons were prepared from corncobs by an initial hydrothermal treatment using ammonium chloride as a pore forming additive and then by KOH activation. Samples were characterized by SEM, XRD, TG analysis and nitrogen adsorption. The effects of preparation conditions on the iodine number, yield and their electrochemical performance as supercapacitor electrodes were investigated. Results indicate that NH_4Cl is helpful for the formation of activated carbons with a hierarchical pore structure. The best activated carbon prepared has a good rate performance with a capacitance of 175 $F\cdot g^{-1}$ at 0.5 $A\cdot g^{-1}$ and a capacity retention ratio of 73.0% at 20 $A\cdot g^{-1}$, and a good cycling stability with a specific capacity change from 175 to 173 $F\cdot g^{-1}$ after a 10 000 charge/discharge test.

Key words: Corncob; Hydrothermal method; Ammonium chloride; Activated carbon; Electrochemical performance

Received date: 2018-08-02; *Revised date*: 2018-09-29
Foundation item: National Natural Science Foundation of China (51502108); Foundation of Jilin Provence Development and Reform Commission (2014N145); Development Project of Science and Technology of Jilin Province (20150520016JH).
Corresponding author: YANG Xiao-min, Ph. D, Associate Professor. E-mail: xmyang@jlu.edu.cn
Author introduction: WEI Qing-ling, Master, Associate Professor. E-mail: wqlrose1999@163.com
English edition available online ScienceDirect (http://www.sciencedirect.com/science/journal/18725805).
DOI: 10.1016/S1872-5805(18)60348-8

1 Introduction

The activated carbon has been widely used as adsorbents[1,2], catalytic materials[3-5], energy and gas storage materials[6-9] and biological materials[10-12] owing to its high specific surface area, strong resistant to acid and alkali corrosion, a certain electrical conductivity and chemical stability. Activated carbon was first made from coal[13,14] and wood[15,16], with the intensification of the energy crisis, coal and wood are no longer the best raw materials for the preparation of activated carbon. Biomass wastes such as corncob[10,17], corn stalk[18,19], rice husk[20,21], rice straw[22,23], peanut skin[2,24,25] and leaves of willow[26], have attracted much attention of researchers, and they are widely used to prepare activated carbons. As a main waste of the agricultural production, corncob is mainly composed of cellulose, lignin and hemicelluloses that can be hydrolyzed to produce xy-

lose[27,28], the raw material for the production of xylitol[29-31] and furfural[32-34]. It is difficult to separate cellulose and lignin from hydrolysis residue, so it is a better choice to use the residue of corncob hydrolysis for the production of activated carbon.

In this paper, the activated carbons were prepared by a two-step method, hydrolysis of corncob and activation of residue. During hydrolysis, NH_4Cl was used as pore forming additive to prepare activated carbons whose iodine value and yield were improved by optimizing the preparation conditions. The effect of NH_4Cl on the structure and electrochemical properties of as-prepared activated carbons was investigated.

2 Experimental

2.1 Materials

The corncob purchased from Jilin province of China was crushed into grain size of approximate 1 cm, ground into powder with the particle size less than 80 mesh and dried to a constant weight at 105 ℃.

2.2 Preparation of activated carbons

2.2.1 Hydrothermal treatment of corncob

10 g dried corncob powder, 50 mL demonized water and a certain amount of ammonium chloride were added to a hydrothermal reactor, stirred into a paste, shocked for 15 min with ultrasonic vibration, and put into an oven for hydrothermal treatment. The product was removed, filtered, washed, and dried to constant weight at 120 ℃ after hydrothermal treatment.

2.2.2 Preparation of activated carbons

A certain amount of the product from hydrothermal treatment was mixed with KOH solutions at different ratios (KOH/hydrothermal product) and equivalent-volume impregnated for 0.5 h at room temperature. The mixture was heated at 120 ℃ to remove surface moisture and put into a high temperature furnace, where temperature was increased from room temperature to 700 ℃ at a rate of 10 ℃ · min^{-1} and then held for 1 h. When the furnace was cooled down to room temperature, the sample was ground into powder, washed with deionized water until the pH of the solution is 7, and dried at 120 ℃ for 3 h. The sample prepared without hydrothermal process was named AC_1, the sample prepared without adding NH_4Cl in hydrothermal process is named AC_0, and the sample made with an addition of 0.5 g NH_4Cl during the hydrothermal process is named AC.

2.3 Characterization of activated carbons

The iodine number used to test the adsorption performance of the activated carbons was determined by reference to the national standard 12496.8-1999 GB/T(China). A mini II surface area and adsorption analyzer was used for nitrogen adsorption-desorption at 77 K. The samples were pretreated at 573 K for 3 h before measuring adsorption isotherms. The specific surface area was calculated from the isotherms using the Brunauer-Emmett-Teller (BET) equation. The MP-plot method was used to calculate the micropore volume. The X-ray powder diffraction (XRD) patterns of the different activated carbons were collected by a D8 FOCUS X-ray powder diffractometer (Bruker company, Germany), using Cu target ($K\alpha$ = 0.154 18 nm). The morphology of samples was observed by a JSM-6490LV scanning electron microscope (SEM). The thermo gravimetric analysis (SDT-Q600) was used to test the thermal stability of samples and raw materials.

2.4 Calculation of the yield of activated carbon

The yield of activated carbon was calculated using the following formula.

$$Y(\%)=\frac{m_2}{m_1}\times 100 \qquad (1)$$

In the formula, Y is the yield of activated carbon (%), m_1 is the mass of the corncob (g) and m_2 is the mass of the activated carbon (g).

2.5 Electrode preparation and electrochemical measurements

The working electrodes were prepared as follows. 85 mg of activated carbon, 10 mg acetylene black and 7 μL polytetrafluoroethylene were mixed in 40 mL ethanol, stirred and heated until the solvent was evaporated completely. The resulting sample was rolled into pieces and cut into a square of 1 cm^2. The pieces were pressed onto nickel foam with a pressure of 10 MPa and dried for 12 h at 80 ℃.

The electrochemical performance was measured in a 6 M KOH solution as the electrolyte. A CHI 660e electrochemical workstation was used to characterize the electrochemical performance of the electrode materials with cyclic voltammetry (CV) tests between 0-1 V at different scan rates of 5-200 mV · s^{-1}. The galvanostatic charge-discharge (GCD) tests were measured at different current densities of 0.5-20 A · g^{-1} in a voltage range of 0.01-1.01 V. The cycle life test was carried out at a current density of 1 A · g^{-1}. The specific capacitance of activated carbons was calculated using the following formula:

$$C=\frac{2I\Delta t}{m\Delta V} \qquad (2)$$

Where C is the specific capacitance of electrode (F · g^{-1}), I is the discharge current (A), Δt is the discharge time (s), m is the mass of activated carbon in the working electrode (g), and ΔV is the potential

difference of discharge process (V).

The button cell made of the two electrodes with the same mass of activated carbon in each electrode in a 6 mol/L KOH solution was used to measure the cycle life of the supercapacitor.

3 Results and discussion

3.1 Effects of the preparation conditions

The effects of the preparation conditions of activated carbons including dosage of NH_4Cl, time and temperature of hydrothermal treatment, and the ratio of KOH to hydrothermal product on the iodine number and yield of activated carbons were investigated (Fig. 1). Fig. 1a reveals that the iodine number and yield of activated carbons increase with increasing the dosage of NH_4Cl, and reach a maximum when the dosage of NH_4Cl is 0.5 g. The results reveal that the addition of NH_4Cl is helpful to increase the adsorption performance of activated carbon and its yield. The effects of hydrothermal time and temperature on iodine number and yield of activated carbon (Fig. 1b and Fig. 1c) indicate that the optimal hydrolysis condition is at 160 ℃ for 5 h. Fig. 1d shows that the iodine number rises but the yield decreases with the mass ratio of KOH to hydrothermal product. The reason may be due to the consumption of hydrothermal product by excess alkali during activation according to the activation mechanism[35,36].

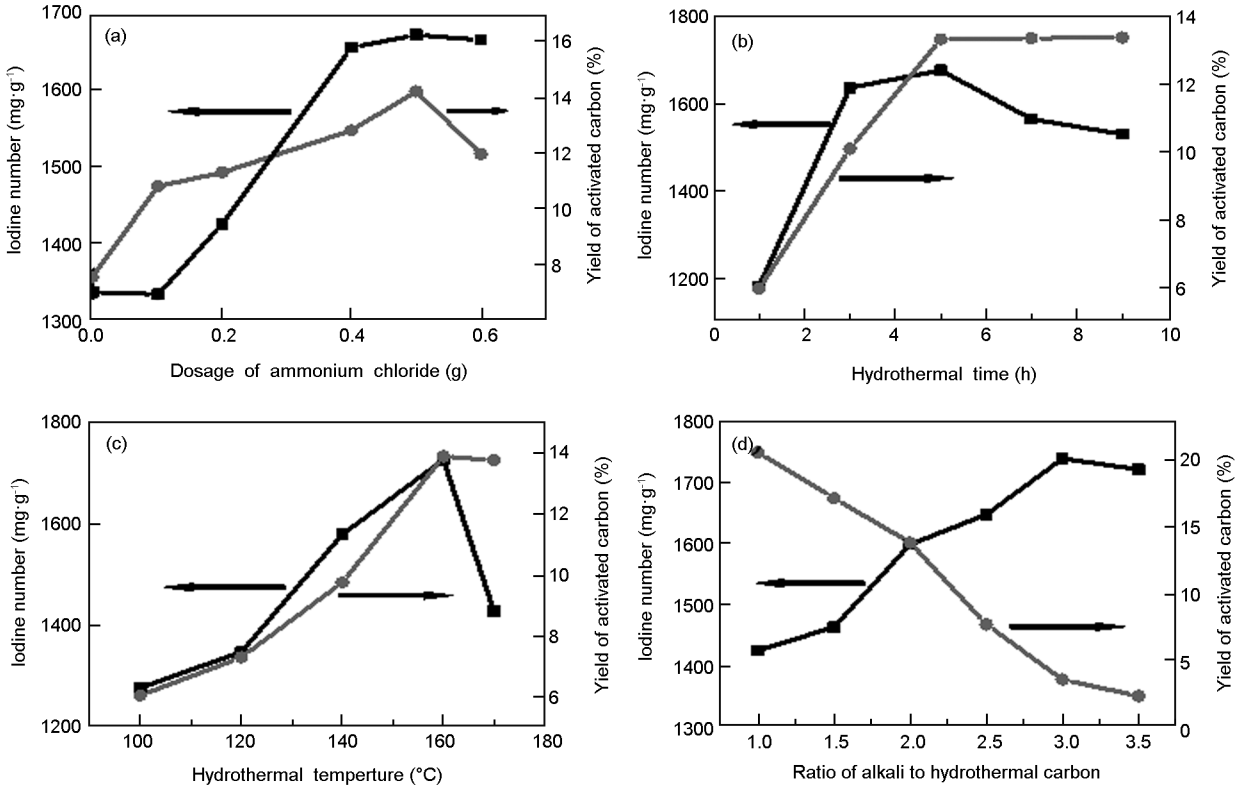

Fig. 1 The effect of preparation conditions on iodine number and yield of activated carbons. (a) Dosage of ammonium chloride, (b) hydrothermal time, (c) hydrothermal temperature and (d) the mass ratio of alkali to hydrothermal product.

3.2 Structure characterization of activated carbons

The X-ray diffraction (XRD) patterns of activated carbos are shown in Fig. 2a, in which the diffraction pattern of AC_1 sample shows only one peak at 26° that are considered as the typical characteristic peak of the amorphous structure of activated carbon. Whereas, the AC_0 and AC samples demonstrate two peaks at 26° and 43°, respectively. The latter corresponds to (100) reflection, indicating the increased graphitization degree [37].

Thermogravimetric (TG) curves (Fig. 2b) of the corncob (CC), hydrothermal carbon (HC) and activated carbon (AC) indicate that the thermal stability of raw materials is increased after hydrothermal treatment, and the weight-loss of activated carbon happens at 650-850 ℃.

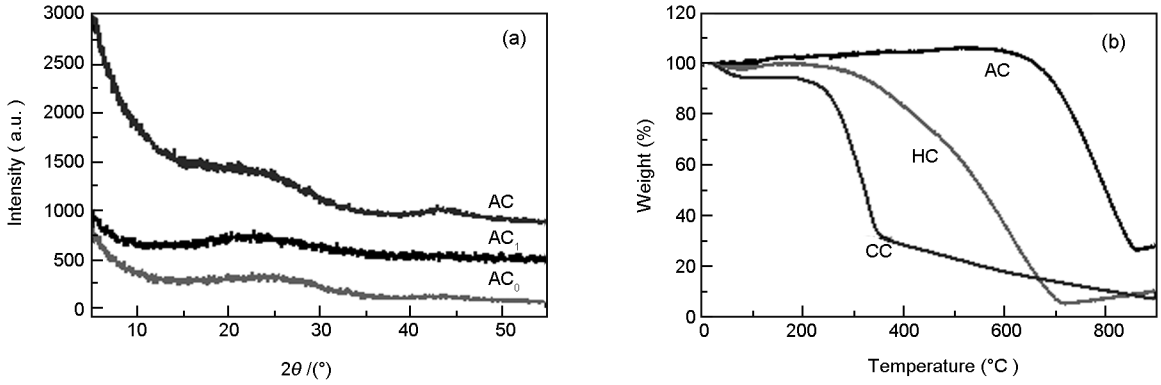

Fig. 2　(a) XRD patterns of activated carbon samples and (b) TG curves of corncob (CC), hydrothermal carbon (HC) and activated carbon (AC).

The morphology of activated carbons was observed by SEM in the Fig. 3, which shows that AC_0 sample has a regular structure of frost flower, while AC sample shows a honeycomb structure with holes of different sizes. The reasons for the formation of holes may be due to the hydrolysis of hemicelluloses with the effect of ammonium chloride, which leads to a loose structure of activated precursor and the formation of the honeycomb holes.

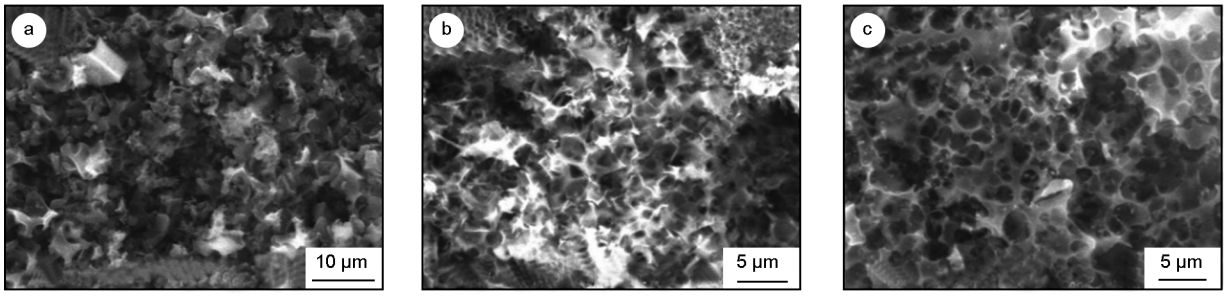

Fig. 3　SEM images of activated carbon samples of (a) AC_1, (b) AC_0 and (c) AC.

The N_2 adsorption-desorption isotherms (Fig. 4) show that AC_1 and AC_0 samples display the type I isotherm based on the IUPAC classification, in which the adsorption isotherm increases rapidly at low pressure zone and then appears a platform at middle and high pressure zone. While, the adsorption-desorption isotherms of AC sample show characteristics similar to the Ⅳ type curve. In the low pressure zone, the adsorption-desorption curves are steep. But a significant hysteresis loop appearing at middle and high pressure zone reveals the presence of mesoporous and macroporous structures [38]. The pore structure parameters (Table 1) show that the AC sample has the biggest BET surface area, total pore volume and average pore diameter, but its ratio of micropore volume to total pore volume is smallest (53.06%) among the three samples. The pore structure parameters imply that the activated carbon prepared by using ammonium chloride as an additive has a hierarchical porous structure[39, 40], which consists of micropores, mesopores and macropores. This kind of structure can not only offer abundant adsorption sites, but also reduce ion diffusion resistance [41,42], which will improve its electrochemical properties.

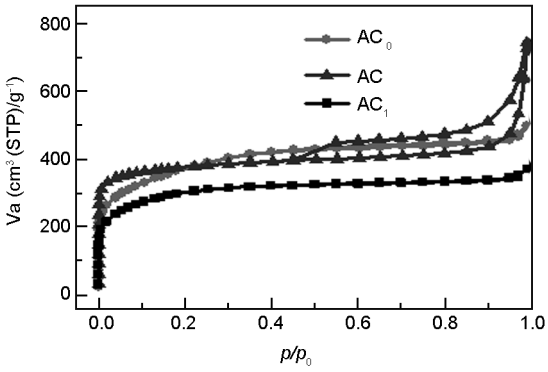

Fig. 4　Nitrogen adsorption-desorption isotherms of activated carbons.

Table 1 Texture properties of activated carbons.

Sample	S_{BET} ($m^2 \cdot g^{-1}$)	V_t ($cm^3 \cdot g^{-1}$)	V_{mic} ($cm^3 \cdot g^{-1}$)	V_{mic}/V_t (%)	D_{ave} (nm)
AC_1	1095.2	0.5728	0.5130	89.56	2.0920
AC_0	1312.7	0.7658	0.6712	87.65	2.3334
AC	1440.3	1.1468	0.6085	53.06	3.1848

S_{BET}: BET surface area, V_t: Total pore volume, V_{mic}: MP-method micropore volume, D_{ave}: Average pore diameter.

3.3 Electrochemical properties of activated carbons

Fig. 5a shows the CV curves of AC, AC_0 and AC_1 samples as electrodes at a scan rate of 5 $mV \cdot s^{-1}$ with a voltage range from 0 to 1 V. It can be seen that all the CV curves show a typical rectangular characteristics of electric double layer capacitors (EDLC). The curve of AC electrode has the biggest area, which indicates the highest capacitance. It is confirmed that the hierarchical porous structure of the activated carbon prepared by using ammonium chloride as an additive contributes to its increased specific capacitance. Although the specific surface area of AC is relatively close to that of AC_0, the specific capacitance of AC electrode is significantly greater than that of AC_0. It is mainly due to the mesoporous structure of AC electrode, which can reduce the resistance during the electron and ion transport. Fig. 5b shows CV curves of AC electrode at a sweep speed range of 5-200 $mV \cdot s^{-1}$. The CV curves show perfect rectangular shape even at 200 $mV \cdot s^{-1}$, indicating the typical EDLC behavior. The GCD tests employed to analyze the capacitive behavior of AC sample are shown in Fig. 5c with a potential window of 0.01-1.01 V at different current densities of 0.5-20 $A \cdot g^{-1}$. The curves of GCD exhibit an isosceles triangle shape at all the current densities and a decreasing trend of the specific capacitance with the current density. The trend is verified by the curve of the specific capacitance of AC electrode at different current densities (Fig. 5d), in which the specific capacitance decreases from 163 to 119 $F \cdot g^{-1}$ with the current density from 0.5 to 20 $A \cdot g^{-1}$. That is, the capacitance retention is 73.0% at the highest current density. The mesoporous and macroporous structures in the electrode materials provide transporting networks and channels for a large number of electrons and ions at high current densities.

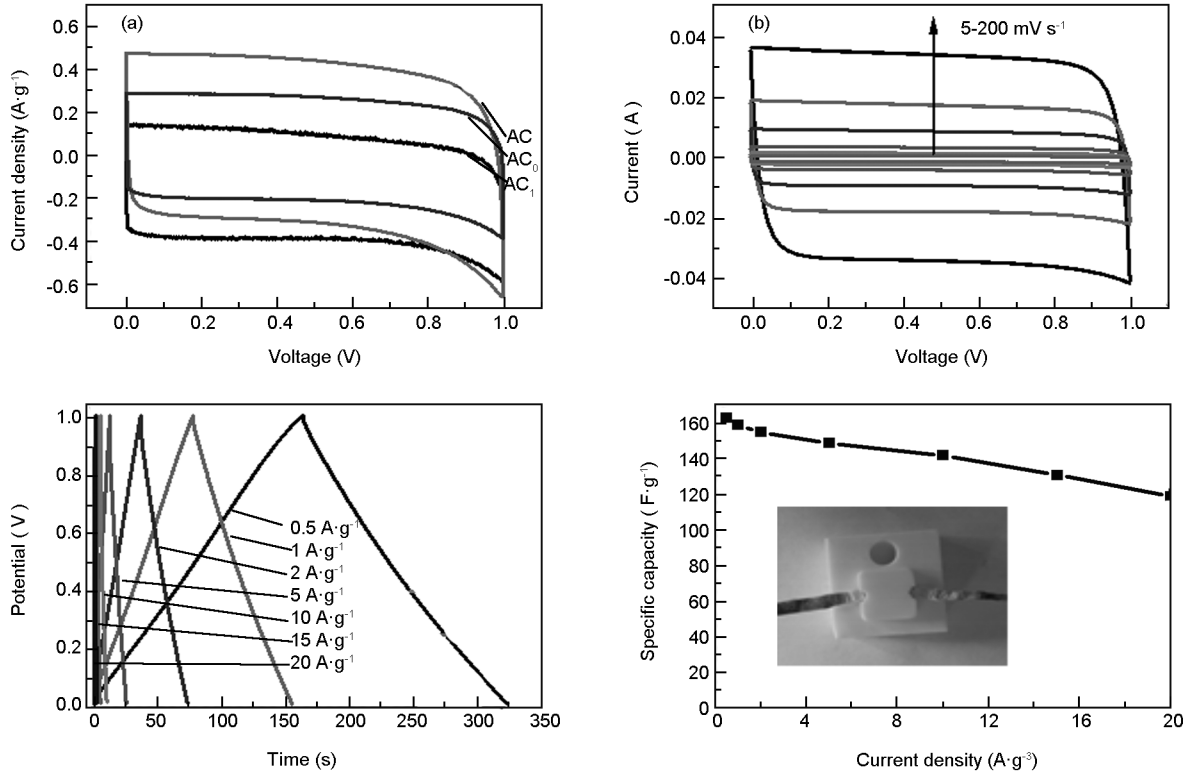

Fig. 5 (a) CV curves of activated carbon electrodes, (b) CV curves of AC electrode at different sweep speeds, (c) GCD curves of AC electrode at different current densities and (d) the specific capacitance of AC electrode at different current densities.

Fig. 6 displays the cycle stability of the AC electrode at a current density of 1 $A \cdot g^{-1}$ and GCD curves at different cycle numbers. The specific capacitance of AC electrode rises from 165 to 175 $F \cdot g^{-1}$ during the first 500 cycles, which could be possibly attributed to the improved wettability and active process of the electrode[43]. During the subsequent cycles of charging and discharging, the specific capacitance of AC electrode reduces from 175 to 173 $F \cdot g^{-1}$, indicating a high capacitance retention of 98.9%. The GCD curves of AC electrode from 4 998 to 10 000 cycles appear almost the same triangular shape, indicating a relatively stable specific capacitance during all the life cycle. The hierarchical porous structure provides unimpeded transport channels for the cyclic stability of AC electrode.

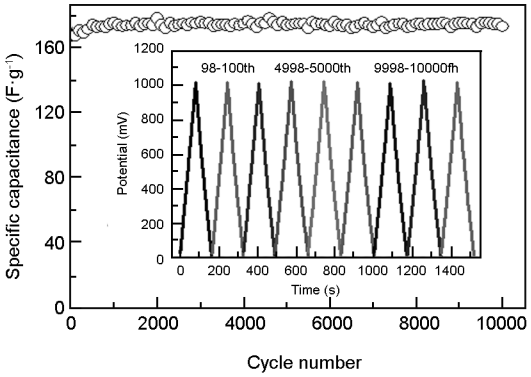

Fig. 6 Cycle stability curve of the AC electrode at the current density of 1 $A \cdot g^{-1}$ and GCD curves of the AC electrode at different cycle numbers.

4 Conclusions

A two step method for preparation high performance corncob-based activated carbons was developed via the hydrothermal process combined with KOH activation using ammonium chloride as a pore forming additive. The use of ammonium chloride increases the yield and iodine number of activated carbons, and it is helpful for the formation of a hierarchical porous structure. As-prepared activated carbon exhibits good electrochemical performance, including a high specific capacitance and long cycle life.

The advantages of the method of for preparation of activated carbon are as following. Firstly, the hydrolysis product can be used as raw material for the production of furfural, so that the biomass resources can be fully utilized. Secondly, compared with the acid hydrolysis of corncob, hydrolysis with ammonium chloride is an environmentally friendly method. Finally, the addition of NH_4Cl as a pore forming additive consumes a relatively small amount of activator during activation.

Acknowledgements

The authors acknowledge the support for characterization of samples from the Center of Analysis Test of Jilin Institute of Chemical Technology.

References

[1] Ahmed M J, Theydan S K. Fluoroquinolones antibiotics adsorption onto microporous activated carbon from lignocellulosic biomass by microwave pyrolysis[J]. J. Taiwan Inst. Chem. Eng., 2014, 45 (1): 219-226.

[2] Larous S, Meniai A-H. Adsorption of diclofenac from aqueous solution using activated carbon prepared from olive stones[J]. Int. J. Hydrogen Energy, 2016, 41 (24): 10380-10390.

[3] Munoz M, Kolb V, Lamolda A, et al. Polymer-based spherical activated carbon as catalytic support for hydrodechlorination reactions[J]. Appl. Catal. B, 2017, 218: 498-505.

[4] Lu S, Liu Y, Feng L, et al. Characterization of ferromagnetic sludge-based activated carbon and its application in catalytic ozonation of p-chlorobenzoic acid[J]. Environ. Sci. Pollut. Res., 2018, 25(6): 5086-5094.

[5] Liu Y, Ning P, Li K, et al. Simultaneous removal of NO_x and SO_2 by low-temperature selective catalytic reduction over modified activated carbon catalysts[J]. Russ. J. Phys. Chem. A, 2017, 91 (3): 490-499.

[6] Li Y F, Liu Y Z, Zhang W K, et al. Green synthesis of reduced graphene oxide paper using Zn powder for supercapacitors[J]. Mater. Lett., 2015, 157: 273-276.

[7] Gao F, Shao G, Qu J, et al. Tailoring of porous and nitrogen-rich carbons derived from hydrochar for high-performance supercapacitor electrodes[J]. Electrochim. Acta, 2015, 155: 201-208.

[8] Qu J, Geng C, Lv S, et al. Nitrogen, oxygen and phosphorus decorated porous carbons derived from shrimp shells for supercapacitors[J]. Electrochim. Acta, 2015, 176: 982-988.

[9] Sawant S Y, Munusamy K, Somani R S, et al. Precursor suitability and pilot scale production of super activated carbon for greenhouse gas adsorption and fuel gas storage[J]. Chem. Eng. J., 2017, 315: 415-425.

[10] Altintig E, Arabaci G, Altundag H. Preparation and characterization of the antibacterial efficiency of silver loaded activated carbon from corncobs[J]. Surf. Coat. Technol., 2016, 304: 63-67.

[11] Ma D, Chen L, Liu R. Removal of novel antiandrogens identified in biological effluents of domestic wastewater by activated carbon[J]. Sci. Total Environ., 2017, 595: 702-710.

[12] Hu Q, Li M, Wang C, et al. Influence of powdered activated carbon addition on water quality, sludge properties, and microbial characteristics in the biological treatment of commingled industrial wastewater[J]. J. Hazard. Mater., 2015, 295: 1-8.

[13] Teng H, Yeh T S, Hsu L Y. Preparation of activated carbon from bituminous coal with phosphoric acid activation[J]. Carbon, 1998, 36 (9): 1387-1395.

[14] Chingombe P, Saha B, Wakeman R J. Surface modification and characterisation of a coal-based activated carbon[J]. Carbon, 2005, 43 (15): 3132-3143.

[15] Gómez-Serrano V, Cuerda-Correa E M, Fernández-González

M C, et al. Preparation of activated carbons from chestnut wood by phosphoric acid-chemical activation. Study of microporosity and fractal dimension [J]. Mater. Lett., 2005, 59 (7): 846-853.

[16] Wang T, Tan S, Liang C. Preparation and characterization of activated carbon from wood via microwave-induced $ZnCl_2$ activation[J]. Carbon, 2009, 47 (7): 1880-1883.

[17] 邢宝林, 陈丽薇, 张传祥, 等. 玉米芯活性炭的制备及其电化学性能研究. 材料导报, 2015, 29 (3): 45-64.
(Xing Bao-lin, Chen Li-wei, Zhang Chuan-xiang, et al. Preparation and electrochemical performance of corncob-based activated carbon[J]. Materials Review, 2015, 29 (3): 45-64.)

[18] Li Y, Li Y, Li L, et al. Preparation and analysis of activated carbon from sewage sludge and corn stalk[J]. Adv. Powder Technol., 2016, 27 (2): 684-691.

[19] Han M, Qu J, Guo Q. Corn stalk activated carbon based Co catalyst prepared by one-step method for hydrogen generation [J]. Procedia Eng., 2015, 102: 450-457.

[20] Liu D, Zhang W, Lin H, et al. A green technology for the preparation of high capacitance rice husk-based activated carbon [J]. J. Cleaner Prod., 2016, 112(1): 1190-1198.

[21] Vu D, Seo J, Lee H, et al. Activated carbon with hierarchical micro-mesoporous structure obtained from rice husk and its application for lithium-sulfur batteries[J]. RSC Adv., 2017, 7 (7): 4144-4151.

[22] Adinaveen T, Vijaya J J, Kennedy L J. Comparative study of electrical conductivity on activated carbons prepared from various cellulose materials[J]. Arabian J. Sci. Eng., 2016, 41 (1): 55-65.

[23] Adinaveen T., Kennedy L J, Vijaya J J, et al. Surface and porous characterization of activated carbon prepared from pyrolysis of biomass (rice straw) by two-stage procedure and its applications in supercapacitor electrodes[J]. J. Mater. Cycles Waste Manage., 2015, 17 (4): 736-747.

[24] Hamza U D, Nasri N S, Amin N S, et al. Characteristics of oil palm shell biochar and activated carbon prepared at different carbonization times[J]. Desalin. Water Treat., 2016, 57 (17): 7999-8006.

[25] Erdogan F O. Characterization of the activated carbon surface of cherry stones prepared by sodium and potassium hydroxide[J]. Anal. Lett., 2016, 49(7): 1079-1090.

[26] Liu Y, Wang Y, Zhang G, et al. Preparation of activated carbon from willow leaves and evaluation in electric double-layer capacitors[J]. Mater. Lett., 2016, 176: 60-63.

[27] Lu Y, Mosier N S. Biomimetic catalysis for hemicellulose hydrolysis in corn stover[J]. Biotechnol. Prog., 2007, 23 (1): 116-123.

[28] Makishima S, Mizuno M, Sato N, et al. Development of continuous flow type hydrothermal reactor for hemicellulose fraction recovery from corncob[J]. Bioresour. Technol., 2009, 100 (11): 2842-2848.

[29] Mikkola J P, Salmi T. Three-phase catalytic hydrogenation of xylose to xylitol prolonging the catalyst activity by means of online ultrasonic treatment[J]. Catal. Today, 2001, 64 (3-4): 271-277.

[30] Mussatto S I, Roberto I C. Xylitol production from high xylose concentration: evaluation of the fermentation in bioreactor under different stirring rates[J]. J. Appl. Microbiol., 2003, 95 (2): 331-337.

[31] De F D, Torre P, Perego P, et al. Statistical investigation on the effects of starting xylose concentraiton and oxygen mass flowrate on xylitol production from rice straw hydrolyzate by response surface methodology[J]. J. Food Eng., 2004, 65 (3): 383-389.

[32] Choudhary V, Pinar A B, Sandler S I, et al. Xylose isomerization to xylulose and its dehydration to furfural in aqueous media [J]. ACS Catal., 2011, 1 (12): 1724-1728.

[33] Dias A S, Pillinger M, Valente A A. Dehydration of xylose into furfural over micro-mesoporous sulfonic acid catalysts[J]. J. Catal., 2005, 229 (2): 414-423.

[34] Binder J B, Blank J J, Cefali A V, et al. Synthesis of furfural from xylose and xylan[J]. ChemSusChem, 2010, 3 (11): 1268-1272.

[35] Lillo-Ródenas M A, Juan-Juan J, Cazorla-Amorós D, et al. About reactions occurring during chemical activation with hydroxides[J]. Carbon, 2004, 42 (7): 1371-1375.

[36] Lillo-Ródenas M A, Cazorla-Amorós D, Linares-Solano A. Understanding chemical reactions between carbons and NaOH and KOH: An insight into the chemical activation mechanism [J]. Carbon, 2003, 41 (2): 267-275.

[37] Liu Y Z, Li Y F, Yuan S X, et al. Synthesis of 3D N, S dual-doped porous carbons with ultrahigh surface areas for highly efficient oxygen reduction reactions[J]. ChemElctroChem, DOI: 10.1002/celc.201800937.

[38] He X, Li X, Ma H, et al. ZnO template strategy for the synthesis of 3D interconnected graphene nanocapsules from coal tar pitch as supercapacitor electrode materials [J]. J. Power Sources, 2017, 340:183-191.

[39] Wang X, Ma H, He X, et al. Fabrication of interconnected mesoporous carbon sheets for use in high-performance supercapacitors[J]. New Carbon Materials, 2017, 32 (3): 213-220.

[40] Liu Y Z, Li Y F, Su F Y, et al. Easy one-step synthesis of N-doped graphene for supercapacitors[J]. Energy Storage Mater, 2016, 2: 69-75.

[41] Pan L, Wang Y, Hu H, et al. 3D self-assembly synthesis of hierarchical porous carbon from petroleum asphalt for supercapacitors[J]. Carbon, 2018, 134: 345-353.

[42] He X, Zhang N, Shao X, et al. A layered-template-nanospace-confinement strategy for production of corrugated graphene nanosheets from petroleum pitch for supercapacitors[J]. Chem. Eng. J., 2016, 297: 121-127.

[43] Zhou J, Lian J, Hou L, et al. Ultrahigh volumetric capacitance and cyclic stability of fluorine and nitrogen co-doped carbon microspheres[J]. Nat. Commun., 2015, 6: 8503.